Teng et al. Nanoscale Research Letters (2018) 13:60
https://doi.org/10.1186/s11671-018-2475-8

Nanoscale Research Letters

NANO EXPRESS Open Access

A Nanocrystalline Fe_2O_3 Film Anode Prepared by Pulsed Laser Deposition for Lithium-Ion Batteries

Xiaoling Teng, Youzhi Qin, Xia Wang, Hongsen Li, Xiantao Shang, Shuting Fan, Qiang Li*, Jie Xu, Derang Cao and Shandong Li*

Abstract

Nanocrystalline Fe_2O_3 thin films are deposited directly on the conduct substrates by pulsed laser deposition as anode materials for lithium-ion batteries. We demonstrate the well-designed Fe_2O_3 film electrodes are capable of excellent high-rate performance (510 mAh g^{-1} at high current density of 15,000 mA g^{-1}) and superior cycling stability (905 mAh g^{-1} at 100 mA g^{-1} after 200 cycles), which are among the best reported state-of-the-art Fe_2O_3 anode materials. The outstanding lithium storage performances of the as-synthesized nanocrystalline Fe_2O_3 film are attributed to the advanced nanostructured architecture, which not only provides fast kinetics by the shortened lithium-ion diffusion lengths but also prolongs cycling life by preventing nanosized Fe_2O_3 particle agglomeration. The electrochemical performance results suggest that this novel Fe_2O_3 thin film is a promising anode material for all-solid-state thin film batteries.

Keywords: Lithium-ion batteries, Nanocrystalline Fe_2O_3, Anode material

Background

With the ever-increasing applications of lithium-ion batteries (LIBs) in portable electronics and electric vehicles, there has been extensive research on developing advanced electrode materials with higher energy and power densities [1–7]. Since the first report on reversible lithium storage in transition metal oxides (TMOs) by Poizot et al. [8], TMOs (Co_3O_4 [9, 10], NiO [11, 12], Fe_2O_3 [13–15], and CuO [16, 17]) have been widely explored as anode materials due to their higher theoretical specific capacity and better safety in comparison with traditional carbon anode materials. Among all these TMOs, Fe_2O_3 received much attention in recent years due to its high theoretical specific capacity (~ 1005 mAh g^{-1}), low cost, abundant resources, and environmental benignity. However, like other TMOs, the huge volume variations associated with Li-ion insertion/extraction often leads to the pulverization and subsequent falling off of the active materials from the electrode, which results in a significant capacity fade, poor cycling stability, and poor rate capability. To circumvent these problems, many nanostructures of Fe_2O_3 have been synthesized for lithium-ion batteries, such as nanorods [18, 19], nanoflakes [20, 21], hollow sphere [22–24], core-shell arrays [25], and micro-flowers [26].

Besides all the above nanostructures, nanocrystalline thin film anodes (NiO [27], MnO [28], Cr_2O_3 [29], $CoFe_2O_4$ [30], Si [31], and Ni_2N [32]) deposited directly on conducting substrates by pulsed laser deposition or sputtering can also exhibit an excellent electrochemical performance due to the enhanced electrical contact between the substrates and active materials, the shortened diffusion lengths for lithium-ion, and the structure stability. What is more important is that thin films of TMOs have potential applications in all-solid-state microbatteries as self-supported electrodes [33, 34]. The TMOs' films can replace the lithium film anode which limits the integration of microbatteries with circuits due to the low melting point and strong reactivity with moisture and oxygen. However, up to now, there have been few reports on the Fe_2O_3 film anodes deposited by pulsed laser deposition or sputtering, and the reported specific capacities were much lower than the theoretical specific capacity of Fe_2O_3 [35, 36].

* Correspondence: liqiang@qdu.edu.cn; lishd@qdu.edu.cn
College of Physics Science, Qingdao University, No.308 Ningxia Road, Qingdao 266071, China

In this work, we prepared nanocrystalline Fe_2O_3 films by pulsed laser deposition (PLD) as an anode material for lithium-ion batteries. The Fe_2O_3 thin film anodes with average grain size of several tens of nanometers showed high reversible capacity of 905 mAh g^{-1} at 100 mA g^{-1} and high rate capacity of 510 mAh g^{-1} at 15000 mA g^{-1}. The remarkable electrochemical performance demonstrates that nanocystalline Fe_2O_3 thin film has potential applications in high performance LIBs, especially all-solid-state thin film batteries.

Experimental

Synthesis of Nanocrystalline Fe_2O_3 Films

The films of Fe_2O_3 were deposited directly on copper foils or stainless steels by a PLD technique in oxygen ambient. A KrF excimer laser with a wavelength of 248 nm was focused on the rotatable target of metal Fe. The repetition rate was 5 Hz, and the laser energy was 500 mJ. The distance between the target and the substrate was 40 mm. In order to get nanocrystalline Fe_2O_3 films, we grew samples at room temperature under oxygen pressure of 0.3 Pa on both copper foil and stainless steels. They showed the same electrochemical performance. The thickness of the nanocomposite film is approximately 200 nm as determined by atomic force microscope (AFM, Park systems XE7). The mass of 0.121 mg was obtained by measuring the difference of substrate before and after deposition via electrobalance (METTLER TOLEDO).

Material Characterization

The crystalline phase of the Fe_2O_3 film was characterized by X-ray diffraction (XRD) on a Rigaku D/Max diffractometer with filtered Cu Kα radiation ($\lambda = 1.5406$ Å) at a voltage of 40 kV and a current of 40 mA. High-resolution transmission electron microscopy (TEM) and selected area electron diffraction (SEAD) were carried out by a JEOL 100CX instrument. For the TEM measurement, the Fe_2O_3 film grown on NaCl substrate was put into water to dissolve the NaCl. After that, the suspension was dropped onto a holey carbon grid and dried. The morphology of the samples were observed by scanning electron microscopy (SEM) using a SU8010. X-ray photoelectron spectroscopy (XPS) measurement was performed on a Thermo Scientific ESCALAB 250XI photoelectron spectrometer.

Electrochemical Measurements

For the electrochemical measurements, conventional CR2032 type coin cells with the Fe_2O_3 nanocrystalline film anodes were assembled inside an argon-filled glove box with the oxygen and moisture content below 0.1 ppm. The electrochemical cells were prepared using lithium metal as the counter electrode and a standard electrolyte of 1:1:1 ethylene carbonate (EC)/dimethyl carbonate (DMC)/$LiPF_6$. Galvanostatic cycling measurements were processed at room temperature by a LAND-CT2001A battery system at various current rates between 0.01 and 3.0 V. Cyclic voltammetry (CV) and AC impedance measurements were performed with a CHI660E electrochemical workstation (CHI Instrument TN). The scanning rate was 0.1 mV s^{-1}.

Results and Discussion

X-ray diffraction (XRD) patterns of the Fe_2O_3 film are shown in Fig. 1a. It can be observed that there is no obvious peak except the peaks of cubic crystal Cu substrate, suggesting that the Fe_2O_3 film is amorphous or crystallized with nanosized grains. Such phenomenon could be attributed to the deposition occurred at room temperature. In order to determine the chemical composition of the obtained film, XPS measurement was performed as shown in Fig. 1b. The Fe $2p_{3/2}$ and Fe $2p_{1/2}$ main peaks are clearly accompanied by satellite structures on their high binding-energy side, with a relative shift of about 8 eV. The peaks of Fe $2p_{3/2}$ locating at 710.9 eV and Fe $2p_{1/2}$ locating at 724.5 eV are similar with XPS spectra of Fe_2O_3 reported in

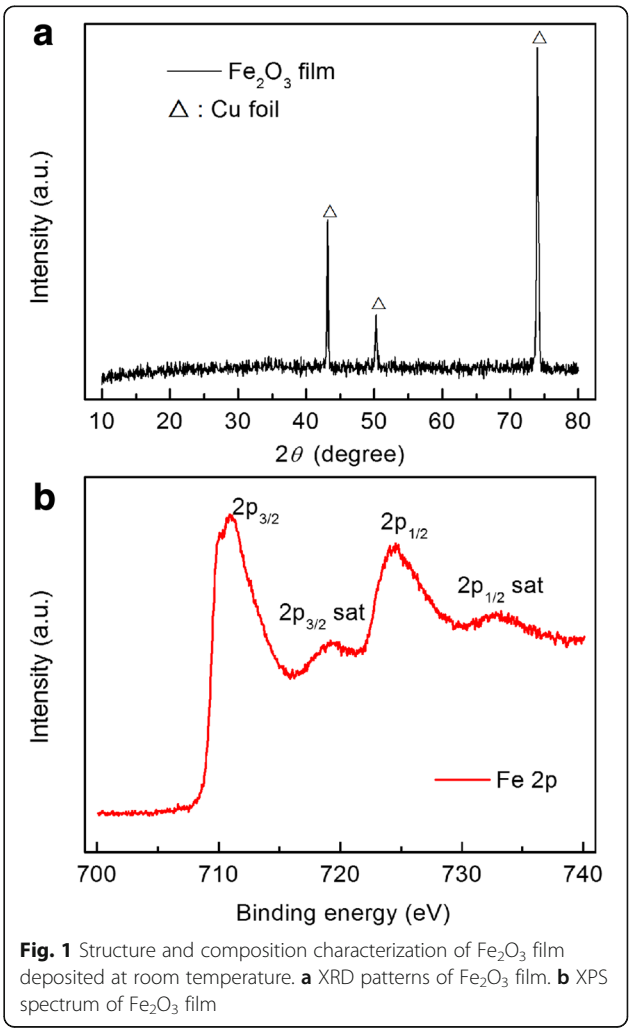

Fig. 1 Structure and composition characterization of Fe_2O_3 film deposited at room temperature. **a** XRD patterns of Fe_2O_3 film. **b** XPS spectrum of Fe_2O_3 film

the literature [37–39]. To further reveal the structure and composition of as-deposited thin films, TEM characterization was conducted as shown in Fig. 2. It revealed that the Fe_2O_3 films were made of small nanograins with average size of several tens of nanometers. The HRTEM image clearly presents the lattice fringes of the (110) corresponding to d-spacing of 0.251 nm of α-Fe_2O_3. Meanwhile, the ring-like feature of the selected area electron diffraction (SAED) confirmed the polycrystalline nature of Fe_2O_3 film. As shown by the SEM images in Fig. 2c, the Fe_2O_3 film consists of particles in nanometer scale. Based on all these results, we can confirm that the film deposited at room temperature is composed of Fe_2O_3 with ultrafine nanosized crystalline grains.

The electrochemical performance of the electrode made of Fe_2O_3 nanocrystalline film was firstly evaluated by cyclic voltammetry (CV). Figure 3 shows the first three CV curves of Fe_2O_3 nanocrystalline film anode. The CV curves are similar to the previous reports of Fe_2O_3 anode [40–46]. In the first cathodic process, three peaks were observed at 1.38, 1.02, and 0.84 V, which could be related to a multi-step reaction. First, the very small peak at 1.38 V may be due to the lithium insertion into the crystal structure of Fe_2O_3 film forming $Li_xFe_2O_3$ without change in the structure [40, 43]. Second, another peak at about 1.02 V could be ascribed to phase transition from hexagonal $Li_xFe_2O_3$ to cubic $LiFe_2O_3$. The third sharp reduction peak at 0.84 V corresponds to the complete reduction of iron from Fe^{2+} to Fe^0 and the formation of solid electrolyte interface (SEI). In the anodic process, two broad peaks observed at 1.57 and 1.85 V represent the oxidation of Fe^0 to Fe^{2+} and further oxidization to Fe^{3+}. In the subsequent cycles, the reduction peaks were replaced by two peaks locating around 0.88 V because of the irreversible phase transformation in the first cycle. The overlapping of the CV curves during the following 2 cycles demonstrated good reversibility of the electrochemical reactions, and this was further confirmed by the cycling performance.

Figure 4a shows the discharge and charge profiles of the Fe_2O_3 nanocrystalline film for different cycles at a specific current of 100 mA g^{-1} with a voltage range of 0.01–3 V. Obvious voltage hysteresis are observed due to the conversion reaction during charge/discharge processes, and the voltage plateaus are in good agreement with the above CV results. The clear voltage slopes observed in each charge/discharge process indicate the oxidation of Fe to Fe^{3+} and the reduction of Fe^{3+} to Fe, respectively. The smooth slope from 1.5 to 2.0 V in the charge process represents the two oxidation peaks in the CV curves. Meanwhile, the plateau or slope around 0.9 V in the discharge process represents the reduction peak in the CV curves. The initial discharge and discharge capacity of the Fe_2O_3 nanocrystalline film are 1183 and 840 mAh g^{-1},

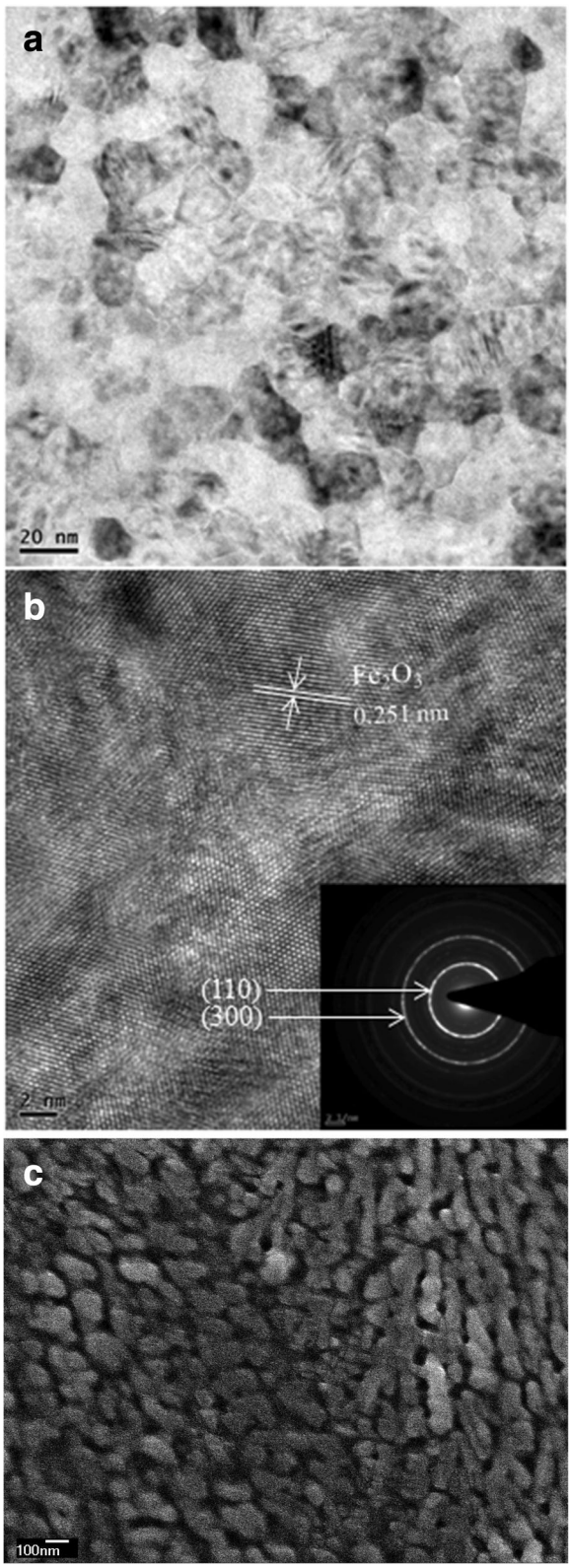

Fig. 2 **a** TEM image. **b** HRTEM image with inset showing SAED patterns. **c** SEM image of the Fe_2O_3 film prepared at room temperature

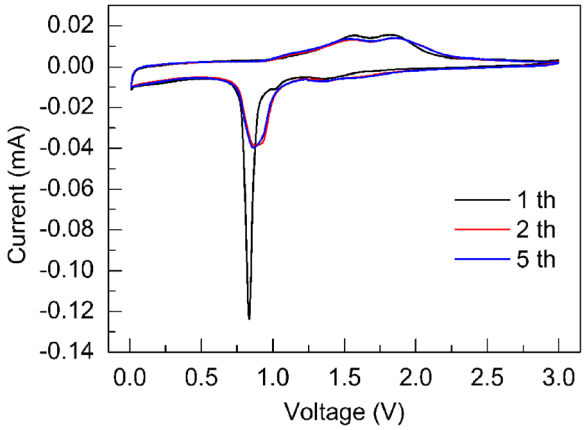

Fig. 3 Cyclic voltammetry curves of the nanocrystalline Fe_2O_3 film. The curves were measured at a scan rate of 0.1 mV s^{-1} from 0.01 to 3 V

respectively, resulting in a Coulombic efficiency of 71%. The irreversible capacity loss is mainly attributed to the formation of SEI layer on the surface of anode, which is commonly observed in most anode materials [44–47].

The cycling performance of the film electrode at a specific current of 100 mA g^{-1} at room temperature is shown in Fig. 4b. It can be seen that the reversible capacity gradually increases to 951 mAh g^{-1} after the 70 cycles and then keeps stable in the range of 900–950 mAh g^{-1} with a Coulombic efficiency nearly 100% during the following cycles. Similar phenomenon of the capacity increasing during cycling has been found in many transition metal oxide electrodes in previous studies [13, 48–52]. The possible reason for this would be the electrode activation, which induces the reversible growth of polymer/gel-like films to increase the capacity at low potentials [50]. Compared with the previous reports of Fe_2O_3 film anode batteries deposited by pulsed laser deposition or sputtering [35, 36], the capacity of Fe_2O_3 in our work has a considerable improvement as summarized in Table 1.

Table 1 The capacity comparison of our work with reported Fe_2O_3 film anode

Fe_2O_3-based thin film anode	Current density	Cycle number	Capacity (mAh g^{-1})	Ref.
Pulsed laser deposition	100 mA g^{-1} 100 mA g^{-1}	200 50	905 361	This work
Pulsed laser deposition	100 μA cm^{-2}	50	280	[35]
Sputter deposition	165 mA g^{-1}	120	330	[36]

Previous studies on the effect of particle size on lithium intercalation into Fe_2O_3 shows that nanocrystalline Fe_2O_3 exhibited better electrochemical performance

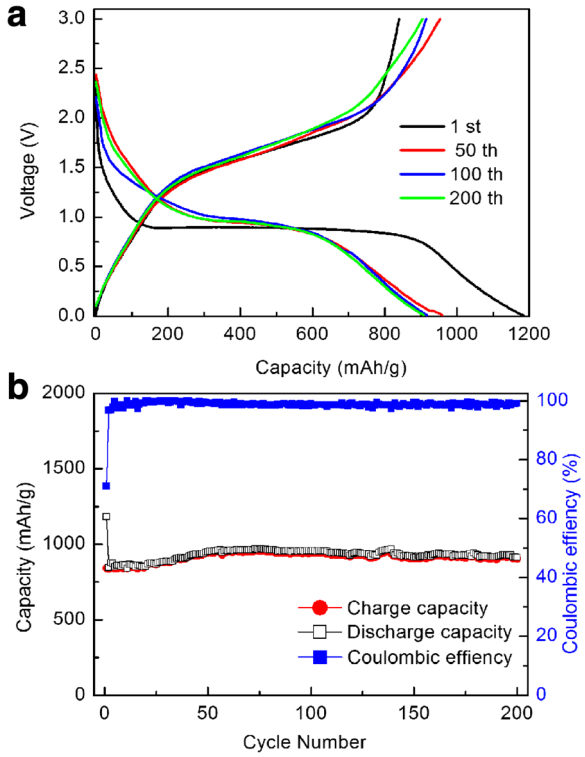

Fig. 4 a Discharge-charge profiles of the nanocrystalline Fe_2O_3 film anode cycled between 0.01–3 V at a specific current of 100 mA g^{-1}. **b** Cycling performance of the nanocrystalline Fe_2O_3 film anode and corresponding Coulombic efficiencies at a specific current of 100 mA g^{-1}

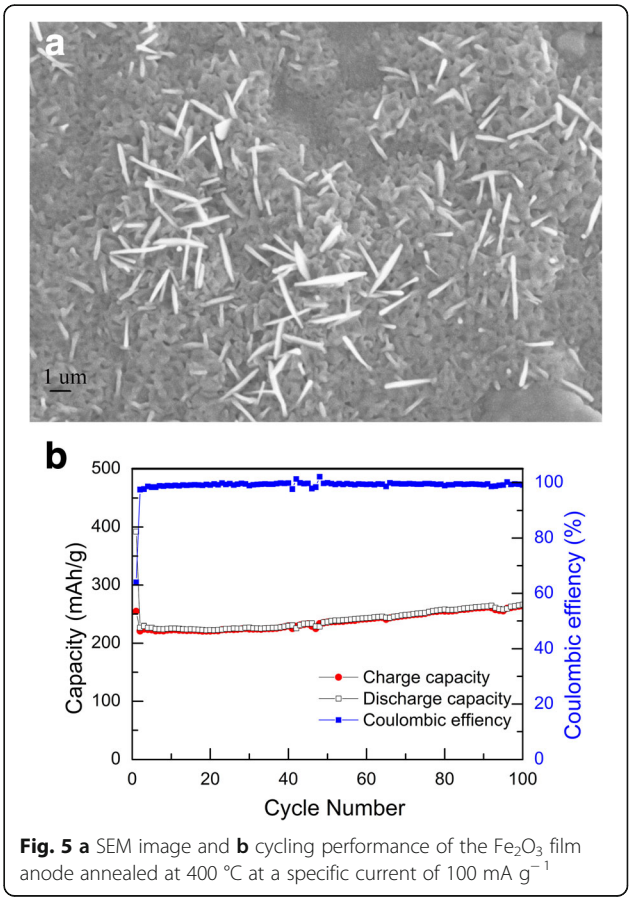

Fig. 5 a SEM image and **b** cycling performance of the Fe_2O_3 film anode annealed at 400 °C at a specific current of 100 mA g^{-1}

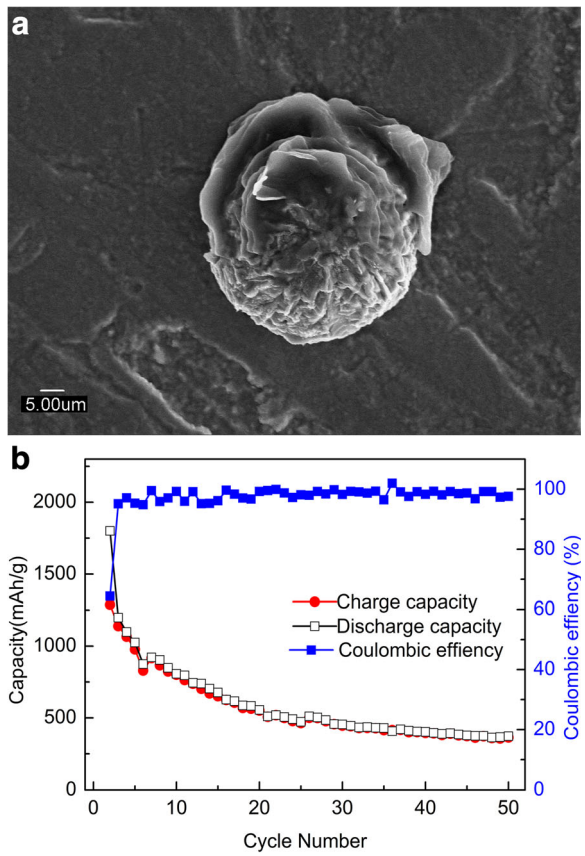

Fig. 6 **a** SEM image and **b** cycling performance of the Fe_2O_3 film anode grown at 400 °C at a specific current of 100 mA g^{-1}

than macro-sized (> 100 nm) Fe_2O_3 [53]. To confirm the role of particle size in the electrochemical performance, we annealed the as-prepared Fe_2O_3 film on stainless steels at 400°. The prepared Fe_2O_3 film anode at high temperature was deposited on stainless steels only due to the instability of copper foil. The morphology comparison in Fig. 5a and Fig. 2c confirms that the particle sizes of the samples annealed at high temperature are obviously larger. Figure 5b shows that the capacities was only about 263 mAh g^{-1} after 100 circles, which was much lower than the specific capacity of as-prepared Fe_2O_3. In addition, we also fabricated Fe_2O_3 film anode with larger particle size on stainless steels under 400 °C as shown in Fig. 6a. Figure 6b shows its discharge and charge profiles for different cycles at a specific current of 100 mA g^{-1}. The capacities dropped to 361 mAh g^{-1} after 50 circles. These results indicate that the enhanced reversible capacity of nanocrystalline Fe_2O_3 film grown at room temperature can be attributed to the nanoscaled structure of the thin film electrode, which can sustain high lithium insertion strain because of the smaller number of atoms and large surface areas within nanoparticles [13, 14, 54].

To investigate the kinetics of lithium inserting/deinserting, electrochemical impedance spectra measurement was performed in Fig. 7a. The charge-transfer impedance on the electrode/electrolyte surface is about 50 Ω, which can be deduced from the single semicircle in the high-middle frequency. The superior conductivity of the film electrode without binder can be attributed to the nanocrystalline structure of the Fe_2O_3 film and the enhanced electrical contact between active anode and substrate. The good conductivity of the nanocrystalline Fe_2O_3 film anode led to excellent rate performance. Figure 7b shows the charge/discharge capacities at different current densities. The anode delivered capacities up to 855, 843, 753, 646, and 510 mAh g^{-1} at high current densities of 750, 1500, 3000, 7500, and 15,000 mA g^{-1}, respectively, which is corresponding to 98.2, 96.7, 87.8, 75.3, and 59.5% retention of the capacity at 250 mA g^{-1} (about 871 mAh g^{-1}). More importantly, when the specific current reduced to 250 mA g^{-1}, the capacity could recover to 753 mAh g^{-1}. The excellent rate performance benefits from both the good conductivity of the anode and the increase of capacity upon cycling.

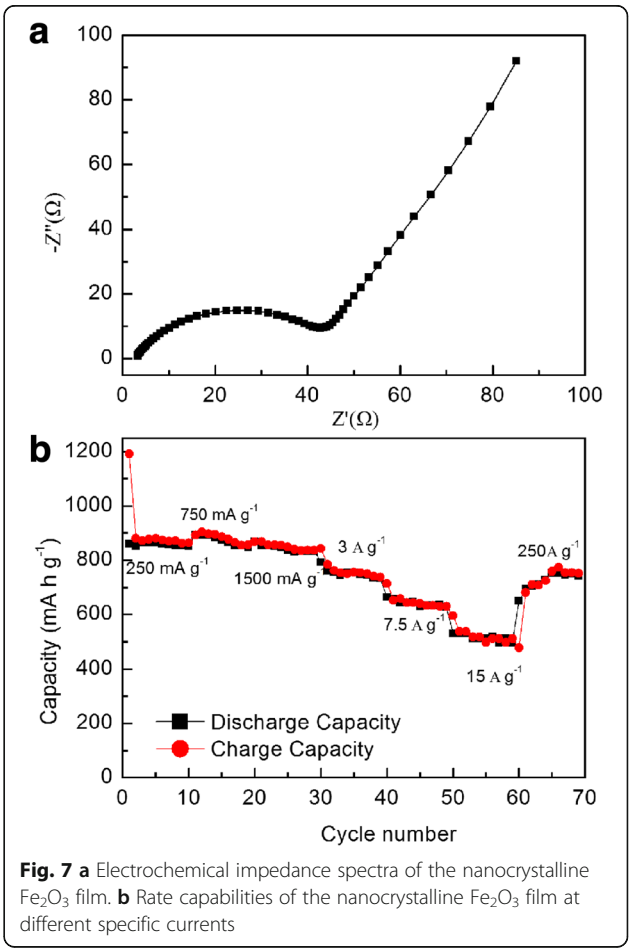

Fig. 7 **a** Electrochemical impedance spectra of the nanocrystalline Fe_2O_3 film. **b** Rate capabilities of the nanocrystalline Fe_2O_3 film at different specific currents

Conclusions

In summary, nanocrystalline Fe_2O_3 film anode has been deposited by pulsed laser deposition at room temperature. The results of structure and morphology characterization showed that the deposited films are composed of nanocrystalline Fe_2O_3 with grain size of several tens of nanometers. The prepared Fe_2O_3 exhibits an excellent electrochemical performance, such as superior cycling stability (905 mAh g^{-1} at a specific current of 100 mA g^{-1} after 200 cycles) and high rate capability (510 mAh g^{-1} at 15000 mA g^{-1}). The outstanding electrochemical performance can be related to the nanocrystalline structure of Fe_2O_3 which could sustain high strain, shorten diffusion lengths for lithium-ion, and keep the structure stable. The excellent electrochemical performance and room temperature growth suggest that nanocrystalline Fe_2O_3 has potential application in high performance LIBs, especially in all-solid-state thin film batteries.

Abbreviations

AFM: Atomic force microscope; CV: Cyclic voltammetry; DMC: Dimethyl carbonate; EC: Ethylene carbonate; LIB: Lithium-ion batteries; PLD: Pulsed laser deposition; SEAD: Selected area electron diffraction; SEI: Solid electrolyte interface; SEM: Scanning electron microscopy; TEM: Transmission electron microscopy; TMOs: Transition metal oxides; XPS: X-ray photoelectron spectroscopy; XRD: X-ray diffraction

Acknowledgements

The authors thank the Institute of Materials for Energy and Environment in Qingdao University for the technical assistance during TEM and SEM observations.

Funding

This work was supported partly by the National Sciences Foundation of China Nos. 11504192, 11674187, 11604172, 11704211; the National Science Foundation of Shandong Province BSB2014010, BS2015SF003; and China Postdoctoral Science Foundation 2015M570570.

Availability of Data and Materials

All data are fully available without restriction.

Authors' Contributions

The experiments and characterization presented in this work were carried out by XLT, YZQ, XTS, and STF. The experiments were designed by QL and SDL. The experiments were discussed in the results by XW, HSL, JX, and DRC. All authors read and approved the final manuscript.

Authors' Information

Not applicable

Competing Interests

The authors declare that they have no competing interests.

Publisher's Note

Received: 27 November 2017 Accepted: 12 February 2018
Published online: 23 February 2018

References

1. Armand M, Tarascon JM (2008) Building better batteries. Nature 451:652–657
2. Goodenough JB, Kim Y (2010) Challenges for rechargeable Li batteries. Chem Mater 22:587–603
3. Tang Y, Zhang Y, Li W, Ma B, Chen XD (2015) Rational material design for ultrafast rechargeable lithium-ion batteries. Chem Soc Rev 44:5926–5940
4. Li H, Peng L, Zhu Y, Chen D, Zhang X, Yu G (2016) An advanced high-energy sodium ion full battery based on nanostructured $Na_2Ti_3O_7$/$VOPO_4$ layered materials. Energy Environ Sci 9:3399–3405
5. Candelaria S, Shao Y, Zhou W, Li X, Xiao J, Zhang J, Wang Y, Liu J, Li J, Cao G (2012) Nanostructured carbon for energy storage and conversion. Nano Energy 1(2):195–220
6. Wang X, Kim HM, Xiao Y, Sun YK (2016) Nanostructured metal phosphide-based materials for electrochemical energy storage. J Mater Chem A 4: 14915–14931
7. Li H, Ding Y, Ha H, Shi Y, Peng L, Zhang X, Ellison C, Yu G (2017) An all-stretchable-component sodium-ion full battery. Adv Mater 29: 1700898
8. Poizot P, Laruelle S, Grugeon S, Dupont L, Tarascon JM (2000) Nano-sized transition-metaloxides as negative-electrode materials for lithium-ion batteries. Nature 407:496–499
9. Wang Y, Pan A, Zhu Q, Nie Z, Zhang Y, Tang Y, Liang S, Cao G (2014) Facile synthesis of nanorod-assembled multi-shelled Co_3O_4 hollow microspheres for high-performance supercapacitors. J Power Sources 272:107–112
10. Wu Z, Ren W, Wen L, Gao L, Zhao J, Chen Z, Zhou G, Li F, Cheng H (2010) Graphene anchored with Co_3O_4 nanoparticles as anode of lithium ion batteries with enhanced reversible capacity and cyclic performance. ACS Nano 4:3187–3194
11. Zhang D, Sun W, Chen Z, Zhang Y, Luo W, Jiang Y, Dou S (2016) Two-dimensional cobalt-/nickel-based oxide nanosheets for high-performance sodium and lithium storage. Chem-Eur J 22:18060–18065
12. Wen W, Wu J, Cao M (2013) Rapid one-step synthesis and electrochemical performance of NiO/Ni with tunable macroporous architectures. Nano Energy 2:1383–1390
13. Jiang Y, Zhang D, Li Y, Yuan T, Bahlawane N, Liang C, Sun W, Lu Y, Yan M (2014) Amorphous Fe_2O_3 as a high-capacity, high-rate and long-life anode material for lithium ion batteries. Nano Energy 4:23–30
14. Zhang H, Zhou L, Yu C (2014) Highly crystallized Fe_2O_3 nanocrystals on graphene: a lithium ion battery anode material with enhanced cycling. RSC Adv 4:495–499
15. Zhao D, Xiao Y, Wang X, Gao Q, Cao M (2014) Ultra-high lithium storage capacity achieved by porous $ZnFe_2O_4$/alpha-Fe_2O_3 micro-octahedrons. Nano Energy 7:124–133
16. Yu W, Zhao JC, Wang MZ, Hu YH, Chen LF, Xie HQ (2015) Thermal conductivity enhancement in thermal grease containing different CuO structures. Nanoscale Res Lett 10:113
17. Mai Y, Wang X, Xiang J, Qiao Y, Zhang D, Gu C, Tu J (2011) CuO/graphene composite as anode materials for lithium-ion batteries. Electrochim Acta 56: 2306–2311
18. Cherian CT, Sundaramurthy J, Kalaivani M, Ragupathy P, Kumar PS, Thavasi V, Reddy MV, Sow CH, Mhaisalkar SG, Ramakrishna S, Chowdari BVR (2012) Electrospun alpha-Fe_2O_3 nanorods as a stable, high capacity anode material for Li-ion batteries. J Mater Chem 22:12198–12204
19. Liu S, Sun Y, Zhou F, Nan J (2016) Improved electrochemical performance of alpha-Fe_2O_3 nanorods and nanotubes confined in carbon nanoshells. Appl Surf Sci 375:101–109
20. Reddy M, Yu T, Sow C, Shen Z, Lim C, Rao GVS, Chowdari BVR (2007) Alpha-Fe_2O_3 nanoflakes as an anode material for Li-ion batteries. Adv Funct Mater 17:2792–2799
21. Tang P, Han L, Genc A, He Y, Zhang X, Zhang L, Galan-Mascaros JR, Morante JR, Arbiol J (2016) Synergistic effects in 3D honeycomb-like hematite nanoflakes/branched polypyrrole nanoleaves heterostructures as high-performance negative electrodes for asymmetric supercapacitors. Nano Energy 22:189–201
22. Wang B, Chen J, Wu H, Wang Z, Lou X (2011) Quasiemulsion-templated formation of alpha-Fe_2O_3 hollow spheres with enhanced lithium storage properties. J Am Chem Soc 133:17146–17148
23. Li C, Hu Q, Li Y, Zhou H, Lv Z, Yang X, Liu L, Guo H (2016) Hierarchical hollow Fe_2O_3@MIL-101(Fe)/C derived from metal-organic frameworks for superior sodium storage. Sci Rep 6:25556
24. Zhu W, Cui X, Liu X, Zhang L, Huang J, Piao X, Zhang Q (2013) Hydrothermal evolution, optical and electrochemical properties of hierarchical porous hematite nanoarchitectures. Nanoscale Res Lett 8:2
25. Luo Y, Luo J, Jiang J, Zhou W, Yang H, Qi X, Zhang H, Fan H, Yu DYW, Li C, Yu T (2012) Seed-assisted synthesis of highly ordered TiO_2@alpha-Fe_2O_3

core/shell arrays on carbon textiles for lithium-ion battery applications. Energy Environ Sci 5:6559–6566
26. Jin S, Deng H, Long D, Liu X, Zhan L, Liang X, Qiao W, Ling L (2011) Facile synthesis of hierarchically structured Fe_3O_4/carbon micro-flowers and their application to lithium-ion battery anodes. J Power Sources 196:3887–3893
27. Cao L, Wang DX, Wang R (2014) NiO thin films grown directly on Cu foils by pulsed laser deposition as anode materials for lithium ion batteries. Mater Lett 132:357–360
28. Cui Z, Guo X, Li H (2013) High performance MnO thin-film anodes grown by radio-frequency sputtering for lithium ion batteries. J Power Sources 244:731–735
29. Khamlich S, Nuru ZY, Bello A, Fabiane M, Dangbegnon JK, Manyala N, Maaza M (2015) Pulsed laser deposited Cr_2O_3 nanostructured thin film on graphene as anode material for lithium-ion batteries. J Alloy Compd 637:219–225
30. Chu Y, Fu Z, Qin Q (2004) Cobalt ferrite thin films as anode material for lithium ion batteries. Electrochim Acta 49:4915–4921
31. Jimenez AR, Klopsch R, Wagner R, Rodehorst UC, Kolek M, Nolle R, Winter M, Placke T (2017) A step toward high-energy silicon-based thin film lithium ion batteries. ACS Nano 11:4731–4744
32. Ma ZY, Zhang H, Sun X, Guo J, Li ZC (2017) Preparation and characterization of nanostructured Ni_2N thin film as electrode for lithium ion storage. Appl Surf Sci 420:196–204
33. Zhou Y, Xue M, Fu Z (2013) Nanostructured thin film electrodes for lithium storage and all-solid-state thin-film lithium batteries. J Power Sources 234:310–332
34. Patil A, Patil V, Shin DW, Choi JW, Paik DS, Yoon SJ (2008) Issue and challenges facing rechargeable thin film lithium batteries. Mater Res Bull 43:1913–1942
35. Li W, Zhou Y, Fu Z (2010) Nanocomposite Fe_2O_3-Se as a new lithium storage material. Electrochim Acta 55:8680–8685
36. Sarradin J, Guessous A, Ribes M (1996) Synthesis and characterization of lithium intercalation electrodes based on iron oxide thin films. J Power Sources 62:149–154
37. Mills P, Sullivan JL (1983) A study of the core level electrons in iron and its three oxides by means of X-ray photoelectron spectroscopy. J Phys D Appl Phys 16:723–732
38. McIntyre NS, Zetaruk DG (1977) X-ray photoelectron spectroscopic studies of iron oxides. Anal Chem 49:1521–1529
39. Brundle CR, Chuang TJ, Wandelt K (1977) Core and valence level photoemission studies of iron oxide surfaces and the oxidation of iron. Surf Sci 68:459–468
40. Sun B, Horvat J, Kim HS, Kim WS, Ahn J, Wang GX (2010) Synthesis of mesoporous alpha-Fe_2O_3 nanostructures for highly sensitive gas sensors and high capacity anode materials in lithium ion batteries. J Phys Chem C 114:18753–18761
41. Chou S, Wang J, Wexler D, Konstantinov K, Zhong C, Liu H, Dou S (2010) High-surface-area alpha-Fe_2O_3/carbon nanocomposite: one-step synthesis and its highly reversible and enhanced high-rate lithium storage properties. J Mater Chem 20:2092–2098
42. Liu H, Wang G, Park J, Wang J, Liu H, Zhang C (2009) Electrochemical performance of alpha-Fe_2O_3 nanorods as anode material for lithium-ion cells. Electrochim Acta 54:1733–1736
43. Qiu J, Li M, Zhao Y, Kong Q, Li X, Li C (2016) Scalable synthesis of nanometric alpha-Fe_2O_3 within interconnected carbon shells from pyrolytic alginate chelates for lithium storage. RSC Adv 6:7961–7969
44. Song Y, Qin S, Zhang Y, Gao W, Liu J (2010) Large-scale porous hematite nanorod arrays: direct growth on titanium foil and reversible lithium storage. J Phys Chem C 114:21158–21164
45. Zhang X, Liu HH, Petnikota S, Ramakrishna S, Fan HJ (2014) Electrospun Fe_2O_3-carbon composite nanofibers as durable anode materials for lithium ion batteries. J Mater Chem A 2:10835–10841
46. Zhu J, Yin Z, Yang D, Sun T, Yu H, Hoster HE, Hng HH, Zhang H, Yan Q (2013) Hierarchical hollow spheres composed of ultrathin Fe_2O_3 nanosheets for lithium storage and photocatalytic water oxidation. Energy Environ Sci 6:987–993
47. Liu H, Zheng Z, Chen BC, Liao LB, Wang X (2017) Cobalt oxide porous nanofibers directly grown on conductive substrate as a binder/additive-free lithium-ion battery anode with high capacity. Nanoscale Res Lett 12:302
48. Yu SH, Lee SH, Lee DJ, Sung YE, Hyeon T (2016) Conversion reaction-based oxide nanomaterials for lithium ion battery anodes. Small 12:2146–2172
49. Ponrouch A, Taberna PL, Simon P, Palacin MR (2012) On the origin of the extra capacity at low potential in materials for Li batteries reacting through conversion reaction. Electrochim Acta 61:13–18
50. Mao Y, Duan H, Xu B, Zhang L, Hu Y, Zhao C, Wang Z, Chen L, Yang Y (2012) Lithium storage in nitrogen-rich mesoporous carbon materials. Energy Environ Sci 5:7950–7955
51. Balaya P, Bhattacharyya AJ, Jamnik J, Zhukovskii YF, Kotomin EA, Maier J (2006) Nano-ionics in the context of lithium batteries. J Power Sources 159:171–178
52. Hu Y, Liu Z, Nam K, Borkiewicz OJ, Cheng J, Hua X, Dunstan MT, Yu X, Wiaderek KM, Du L, Chapman KW, Chupas PJ, Yang X, Grey CP (2013) Origin of additional capacities in metal oxide lithium-ion battery electrodes. Nat Mater 12:1130–1136
53. Larcher D, Masquelier C, Bonnin D, Chabre Y, Masson V, Leriche JB, Tarascon JM (2003) Effect of particle size on lithium intercalation into alpha-Fe_2O_3. J Electrochem Soc 150:A133–A139
54. Wu H, Chen J, Hng H, Lou X (2012) Nanostructured metal oxide-based materials as advanced anodes for lithium-ion batteries. Nano 4:2526–2542